ARTICLE

FXR is a molecular target for the effects of vertical sleeve gastrectomy

Karen K. Ryan[1], Valentina Tremaroli[2], Christoffer Clemmensen[1,3], Petia Kovatcheva-Datchary[2], Andriy Myronovych[4], Rebekah Karns[5], Hilary E. Wilson-Pérez[1], Darleen A. Sandoval[1], Rohit Kohli[4], Fredrik Bäckhed[2,6] & Randy J. Seeley[1]

Bariatric surgical procedures, such as vertical sleeve gastrectomy (VSG), are at present the most effective therapy for the treatment of obesity, and are associated with considerable improvements in co-morbidities, including type-2 diabetes mellitus. The underlying molecular mechanisms contributing to these benefits remain largely undetermined, despite offering the potential to reveal new targets for therapeutic intervention. Substantial changes in circulating total bile acids are known to occur after VSG. Moreover, bile acids are known to regulate metabolism by binding to the nuclear receptor FXR (farsenoid-X receptor, also known as NR1H4). We therefore examined the results of VSG surgery applied to mice with diet-induced obesity and targeted genetic disruption of FXR. Here we demonstrate that the therapeutic value of VSG does not result from mechanical restriction imposed by a smaller stomach. Rather, VSG is associated with increased circulating bile acids, and associated changes to gut microbial communities. Moreover, in the absence of FXR, the ability of VSG to reduce body weight and improve glucose tolerance is substantially reduced. These results point to bile acids and FXR signalling as an important molecular underpinning for the beneficial effects of this weight-loss surgery.

Perhaps surprisingly, the most effective and durable therapies for the treatment of obesity involve surgical, rather than pharmacological or behavioural, intervention. In contrast to the modest impact of diet and exercise, most individuals that lose weight with bariatric surgery maintain reduced levels of body fat for many years[1]. This is associated with considerable improvements in co-morbidities. Notably, 40% of obese type-2 diabetes mellitus patients that undergo bariatric surgery achieve full remission within one year[2]. Despite its efficacy, however, surgery is not an attractive therapeutic option for many individuals suffering from obesity and its consequences. Therefore it is both scientifically and clinically imperative that we identify molecular mechanisms responsible for weight loss and other metabolic improvements so we can target affected pathways in a less-invasive manner.

In the bariatric procedure VSG, approximately 80% of the stomach is removed along the greater curvature. This creates a gastric 'sleeve' in continuity with the oesophagus and duodenum. VSG induces loss of body weight and fat mass, and improves glucose tolerance in humans and in rodents[2,3]. Importantly, the efficacy of VSG is comparable to the more complex Roux-en-Y gastric bypass (RYGB), which not only creates a smaller stomach but also involves surgical re-routeing of the small intestine[4,5]. A recent randomized controlled trial found that VSG and RYGB produced nearly the same remission of type-2 diabetes mellitus after one year, and that both procedures were significantly superior to medical management[2].

Conventional wisdom holds that bariatric surgeries, including VSG and RYGB, lead to weight loss and resolution of type-2 diabetes mellitus directly as a result of reducing the ability of the stomach to physically accommodate a meal. That is, the stomach is made smaller, perhaps imposing a mechanical restriction on the amount of food that can be consumed at one time. Moreover, in RYGB, the flow of nutrients and biliopancreatic secretions is re-routed, perhaps limiting macronutrient absorption. However, growing evidence indicates that restriction and

malabsorption are not the primary mechanisms driving metabolic improvements after bariatric surgery[6]. As just one example, a substantial proportion of diabetic patients are able to stop taking their medications within days of surgery, before substantial weight loss has occurred[2]. Given the short time frame, some controversy exists about the mechanisms underlying this dramatic outcome. Some hypothesize that acute improvements are independent of weight loss and result from changes in gut physiology, including altered neurohumoral signalling or altered microbial ecology. In contrast, others suggest these benefits are the result of the hypocaloric post-operative milieu and rapid weight loss[7,8].

Among the changes to gut physiology that occur following bariatric surgery is altered enterohepatic circulation of bile acids. Both RYGB and VSG are associated with a significant increase in circulating total bile acids in humans and in rodent models[9,10]. It is now clear that, in addition to aiding the mechanical digestion and absorption of lipids, bile acids also bind to FXR to function as signalling molecules contributing to the regulation of various metabolic processes. In light of this role, we hypothesized that FXR-signalling links altered bile acid homeostasis to important post-operative changes in metabolism and gut microbial communities, thereby contributing to the maintenance of weight loss and improvements in glucose control observed following VSG. To test this hypothesis, we applied VSG surgery to diet-induced obese mice with targeted genetic disruption of FXR and their wild-type littermates.

Unbiased pathway analysis

We used sequencing of messenger RNA (mRNA-seq), together with subsequent unbiased pathway analysis, to identify key biological pathways that were altered in the distal small intestine following VSG (Fig. 1). Consistent with our recent report that VSG significantly alters the expression of hepatic genes involved in lipid and bile acid metabolism[9], the pathway 'Nuclear receptors in lipid metabolism and toxicity' emerged as one of the top pathways enriched in genes differentially regulated (fold

[1]Department of Internal Medicine, Division of Endocrinology, Diabetes and Metabolism, University of Cincinnati, Cincinnati, Ohio 45237, USA. [2]Wallenberg Laboratory, Department of Molecular and Clinical Medicine and Sahlgrenska Center for Cardiovascular and Metabolic Research, University of Gothenburg, S-413 45 Gothenburg, Sweden. [3]Department of Drug Design and Pharmacology, Faculty of Health and Medical Sciences, University of Copenhagen, Universitetsparken 2, DK-2100 Copenhagen, Denmark. [4]Department of Pediatrics, Division of Gastroenterology, Hepatology, and Nutrition, Cincinnati Children's Hospital Medical Center, Cincinnati, Ohio 45229, USA. [5]Divison of Biomedical Informatics, Cincinnati Children's Hospital Medical Center, Cincinnati, Ohio 45229, USA. [6]Novo Nordisk Foundation Center for Basic Metabolic Research, Section for Metabolic Receptology and Enteroendocrinology, Faculty of Health Sciences, University of Copenhagen, Copenhagen, DK-2200, Denmark.
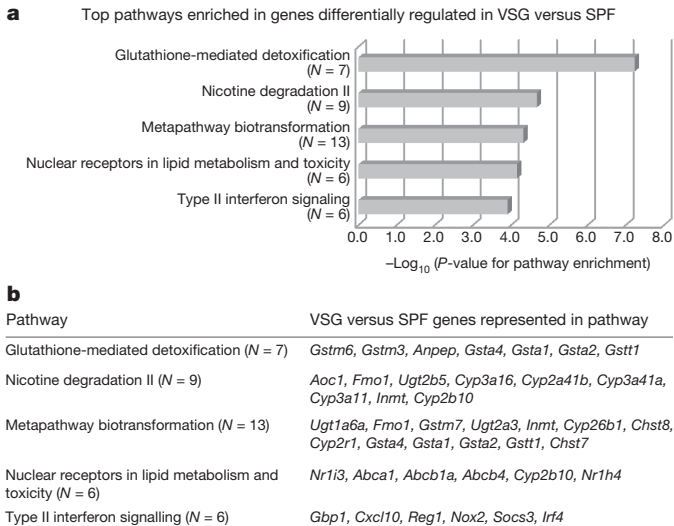
a

Top pathways enriched in genes differentially regulated in VSG versus SPF

b

Pathway	VSG versus SPF genes represented in pathway
Glutathione-mediated detoxification ($N = 7$)	*Gstm6, Gstm3, Anpep, Gsta4, Gsta1, Gsta2, Gstt1*
Nicotine degradation II ($N = 9$)	*Aoc1, Fmo1, Ugt2b5, Cyp3a16, Cyp2a41b, Cyp3a41a, Cyp3a11, Inmt, Cyp2b10*
Metapathway biotransformation ($N = 13$)	*Ugt1a6a, Fmo1, Gstm7, Ugt2a3, Inmt, Cyp26b1, Chst8, Cyp2r1, Gsta4, Gsta1, Gsta2, Gstt1, Chst7*
Nuclear receptors in lipid metabolism and toxicity ($N = 6$)	*Nr1i3, Abca1, Abcb1a, Abcb4, Cyp2b10, Nr1h4*
Type II interferon signalling ($N = 6$)	*Gbp1, Cxcl10, Reg1, Nox2, Socs3, Irf4*

Figure 1 | Unbiased pathway analysis in VSG ileum. a, Based on a pathway analysis of genes differentially regulated (fold change ≥ 1.5) in the terminal ileum of VSG mice relative to sham-operated, pair-fed (SPF) controls, the following top five pathways were significantly enriched as follows: glutathione mediated detoxification ($P = 6.00 \times 10^{-8}$), nicotine degradation ($P = 5.64 \times 10^{-4}$), metapathway biotransformation ($P = 4.81 \times 10^{-5}$), nuclear receptors in lipid metabolism and toxicity ($P = 7.18 \times 10^{-5}$), and type II interferon signalling ($P = 1.25 \times 10^{-4}$). *N*, number of genes differentially regulated in each of the five pathways; $n = 5$ mice per group. **b**, Genes enriched in the five pathways identified in **a**.

change ≥ 1.5) in VSG ($P = 7.18 \times 10^{-5}$). Intriguingly, among the other top pathways, several point towards an altered gut microbiota. Specifically, the glutathione pathway ($P = 6.00 \times 10^{-8}$), which plays important roles in nutrient metabolism and antioxidant defence, is known to be significantly altered by the presence/absence of a microbiota—and this is associated with changes in bile acid composition[11,12]. Likewise, many of the biotransformations ($P = 4.81 \times 10^{-5}$) that are increased probably reflect an altered microbiota, induced for detoxification of metabolites such as secondary bile acids. Finally, changes in gut microbial communities have been extensively linked to altered host immune response including interferon-signalling[13,14] ($P = 1.25 \times 10^{-4}$).

FXR, VSG and body composition

Because we and others have consistently observed increased circulating total bile acids[9,10,15,16] and increased FXR signalling[9,17] following various bariatric procedures including VSG, and because *Fxr* was one of the regulated genes identified in our pathway analysis, we hypothesized that FXR-signalling contributes to the metabolic benefits of VSG. To test this, we first generated whole-body FXR knockout mice (KO), and their wild-type littermate controls (WT; Methods). Because KO mice are somewhat resistant to diet-induced obesity[18], we maintained these mice on a 60% high-fat diet (HFD) for 10 weeks before surgery, such that both WT and KO mice became obese. Both genotypes carried more than 30% of their body weight as fat before surgery (Fig. 2a, b); our previous data indicate that this level of adiposity provides more-than-sufficient opportunity for VSG-induced body weight and fat loss[3,19].

VSG or sham surgery was performed in these obese male WT and KO mice. In the first week after surgery, WT and KO mice lose a comparable amount of weight relative to their sham-operated controls. However, whereas WT-VSG mice maintained this relative weight loss for the duration of the experiment (Fig. 2c, repeated measures analysis of variance (RM ANOVA) with Tukey post-hoc tests, $P < 0.001$), the KO-VSG animals recovered it. Within 5 weeks, the body weight of KO-VSG animals was no longer different from that of sham-operated controls (Fig. 2d, RM ANOVA with Tukey post hoc, $P < 0.001$). Moreover, when we measured body composition at 11 weeks after the operation, WT-VSG mice had half the body fat of sham-operated WT controls, while the body fat of KO-VSG and KO-sham operated mice was equivalent (Fig. 2e, f, two-way ANOVA with Tukey post hoc, $P < 0.01$).

We note that KO-sham mice continue to gain weight at a slower rate than WT-sham mice following surgery; this needs to be taken into consideration. However, the failure of FXR-VSG mice to sustain body weight and body fat loss is unlikely to be a product of KO mice being relatively resistant to diet-induced obesity, for two reasons. First, we have observed potent reductions in body fat after VSG in mice that have as little as an average 7 g of body fat[3,19], whereas the FXR-KO mice in this study had an average of 9 g. Second, we executed post-hoc analyses, selecting the heaviest KO and the lightest WT mice to create a subset with comparable body weights and composition before the surgery. Importantly, in this subset WT-VSG mice maintain an 11.3 g decrement in body weight and a 10.2 g decrement in body fat compared to WT-sham, whereas KO-VSG mice recover to match the body weight and body fat of KO-sham controls within 4–5 weeks. Further, KO-VSG mice are
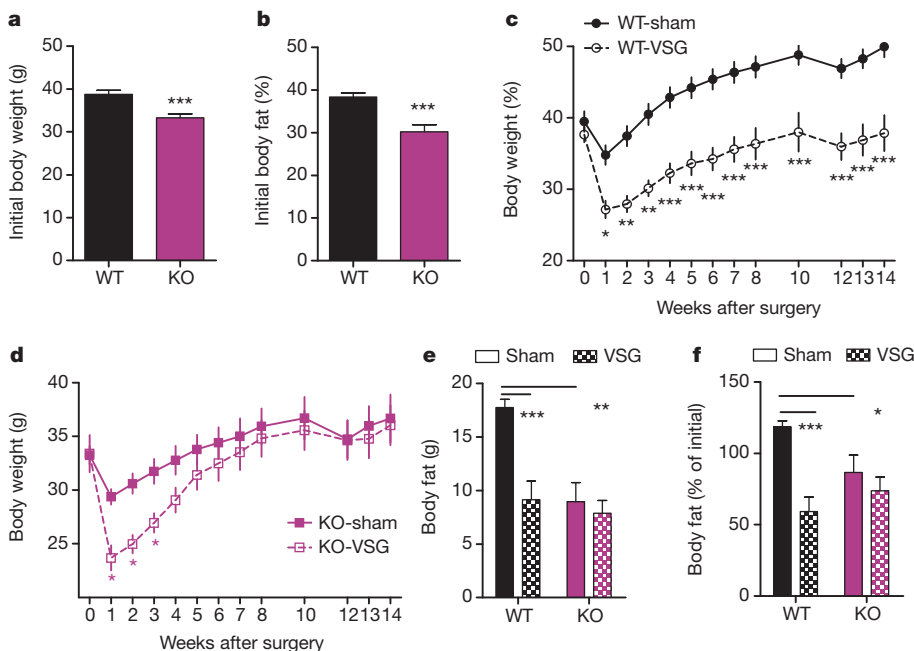

Figure 2 | FXR contributes to the maintenance of weight loss following VSG. a, b, Both WT and FXR KO mice weighed more than 30 g (**a**) and carried more than 30% of their weight as fat (**b**) before the surgery. **c, d**, WT-VSG mice lose weight and maintain this weight loss, relative to WT-sham controls (**c**), whereas KO-VSG mice recover the initial weight loss within 5 weeks after surgery, relative to KO-sham controls (**d**). **e**, 11 weeks after surgery, WT-VSG mice carry half the body fat of WT-sham mice whereas the body fat of KO-VSG and KO-sham mice is equivalent. **f**, 11 weeks after surgery, WT-VSG mice have lost 41% of their pre-surgical body fat, whereas KO-VSG mice exhibit no significant fat loss. Data are shown as mean ± s.e. *$P < 0.05$, **$P < 0.01$, ***$P < 0.001$. For panels **a–d**, $n = 12$ WT-sham, 8 WT-VSG, 9 KO-sham, 8 KO-VSG. For panels **e** and **f**, $n = 12$ WT-sham, 9 WT-VSG, 9 KO-sham, 10 KO-VSG.

significantly heavier than WT-VSG mice by 8 weeks after surgery (Extended Data Fig. 1a–c, two-way ANOVA with Tukey post hoc, $P < 0.001$) and maintain a greater fat mass than WT-VSG mice at 11 weeks after surgery (Extended Data Fig. 1d, e, two-way ANOVA with Tukey post hoc, $P < 0.05$).

FXR, VSG and feeding behaviour

To understand how KO-VSG animals were able to recover this body weight, we measured weekly HFD intake in these singly housed mice. Both WT and KO mice consumed fewer calories during the first week following VSG as compared to sham surgery. However, whereas WT-VSG mice maintained this lower food intake for up to 3 weeks (Fig. 3a, RM ANOVA with Tukey post hoc, $P < 0.001$), KO-VSG mice were only hypophagic during the first week (Fig. 3c, RM ANOVA with Tukey post hoc, $P < 0.001$). Importantly, and in contrast to what occurs when animals are calorically-restricted in the absence of surgery[20], this caloric deficit was not recovered at later time points in WT-VSG mice, allowing for the maintenance of reduced body weight and body fat over the course of the study (Fig. 3a, b). On the other hand, beginning in post-operation week 4, KO-VSG mice actually consumed more food than sham operated controls (Fig. 3c, d, Tukey post hoc $P < 0.05$), suggesting that FXR signalling is necessary for the repression of rebound hyperphagia following caloric restriction initially achieved by VSG. This result is also consistent with our growing understanding that VSG is a metabolic, rather than purely restrictive, procedure[6], as both genotypes are left with a similarly small stomach after VSG.

Eight weeks after surgery, WT-VSG mice had consumed 15% fewer calories than WT-sham mice, but cumulative food intake by KO-VSG mice was equivalent to sham-operated controls (Fig. 3e, two-way ANOVA with Tukey post hoc, $P < 0.01$). Further, when we allowed the mice to choose among three pure macronutrient diets, WT-VSG mice had a significantly reduced preference for fat compared to WT-sham. Unexpectedly, KO-sham mice already exhibit a substantial reduction in the preference for fat compared to WT-sham. This was not further reduced by VSG (Fig. 3f, g, two-way ANOVA with Tukey post hoc, $P < 0.05$). However, we cannot exclude the possibility that the lack of an effect in the KO mice represents a physiological 'floor' that cannot be further reduced by VSG.

FXR, VSG and glucose tolerance

To investigate whether FXR-signalling contributes to improvements in glucose tolerance observed following VSG, we challenged fasted mice with an intraperitoneal (i.p.) injection of dextrose at a dose of 1 g per kg·body weight. VSG was associated with a 20% decrease in fasting

blood glucose in WT mice, whereas it was associated with a 24% increase in fasting blood glucose in KO mice (Fig. 4a, two-way ANOVA with Tukey post hoc, $P < 0.001$). WT-VSG mice exhibited a substantial improvement in the ability to clear the i.p. injection of glucose, reflected as a 35% reduction in the area under the curve (AUC) relative to sham-operated controls. In contrast, KO-VSG and sham-operated mice exhibited no differences in glucose tolerance (Fig. 4b, c, two-way ANOVA with Tukey post hoc, $P < 0.01$; t-test, $P < 0.001$). Although the present findings do not address the question of whether the improvements observed in WT-VSG relative to WT-sham mice are independent of weight loss, we note that KO-VSG and WT-VSG mice had equivalent body weights at the time of this glucose tolerance test. Despite this, when the glucose excursions of WT-VSG and KO-VSG mice are compared directly, KO-VSG mice exhibit significantly impaired glucose clearance at both 30 and 60 min (two-way RM ANOVA with Tukey post hoc, $P < 0.05$, Extended Data Fig. 2).

FXR, VSG and gut microbial communities

Gut microbial communities are altered in obese individuals[21] and respond to changes in caloric intake and macronutrient content of the diet[22]. Recent evidence implicates changes in gut microbial communities, both in humans and mice, as potential contributors to the benefits of weight-loss surgery[23–26]. Transplantation of the gut microbiota from obese mice into germ-free mice is associated with weight gain[27,28], whereas transplantation of gut microbiota from RYGB mice is associated with reduced weight gain compared to transplantation with sham microbiota[26].

Because bariatric surgery affects the prevalence of many microbial species, it has been difficult to ascertain which specific changes might functionally contribute to its benefits. The present study provides an opportunity to address this question, by comparing the interacting effects of FXR deficiency and VSG on gut microbial ecology. Specifically, because FXR KO mice are refractory to the metabolic benefits of VSG, we infer that any changes in gut microbial communities that occur after VSG irrespective of genotype are not sufficient (but may nonetheless be necessary) to recapitulate its benefits. On the other hand, changes that result from an interaction between genotype and surgery are more likely to be critical to the potent effect of VSG. Pertinent to this, bile acids can modulate the abundance and composition of gut microbes, both directly, and indirectly by activation of FXR-signalling[29,30]. Conversely, the gut microbiota can modify bile acid composition by microbial enzymatic activities, thereby altering both bile acid homeostasis and FXR signalling[31,32].

Mice were killed 14 weeks following surgery, and we extracted genomic DNA from caecal contents and performed pyrosequencing of the
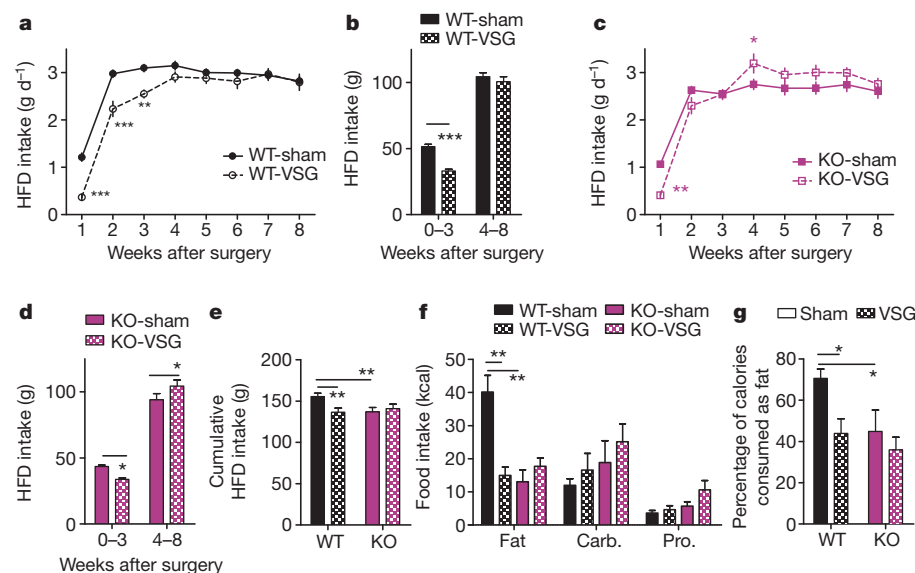

Figure 3 | FXR alters feeding behaviour after VSG. a, b, WT mice eat significantly less during the first 3 weeks after VSG versus sham surgery; this is not recovered at later time points. **c, d,** KO mice eat significantly less during the first week after VSG versus sham surgery; beginning at week 4, KO-VSG mice compensate for this initial caloric deficit by consuming more calories than sham-operated controls. **e,** By 8 weeks after surgery, cumulative food intake by WT-VSG mice was 15% less than WT-sham mice, whereas food intake by KO-VSG and sham-operated mice was equivalent. **f,** When given the choice among three pure macronutrient diets, WT-VSG mice exhibit a blunted preference for dietary fat relative to carbohydrates (Carb.) and protein (Pro.). **g,** Among WT mice, VSG reduces the preference for dietary fat. Moreover, loss of FXR is associated with lack of preference for dietary fat that is not further altered by the surgery. Data are shown as mean ± s.e. *$P < 0.05$, **$P < 0.01$, ***$P < 0.001$. For panels **a–e**, $n = 13$ WT-sham, 10 WT-VSG, 9 KO-sham, 10 KO-VSG. For panels **f, g**, $n = 12$ WT-sham, 6 WT-VSG, 8 KO-sham, 7 KO-VSG.
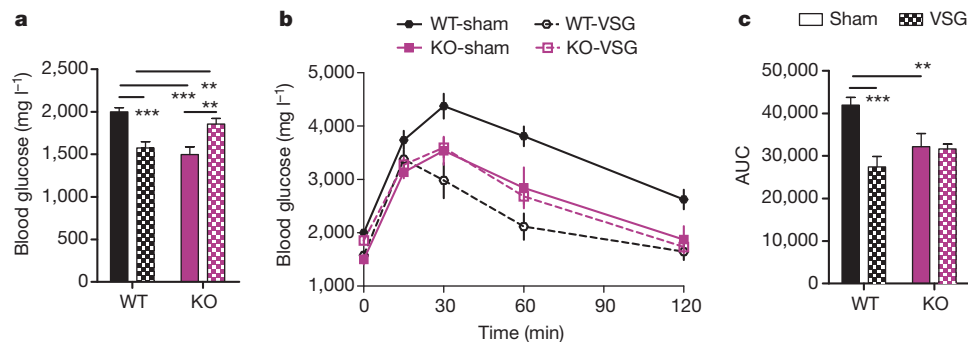
Figure 4 | FXR contributes to the improvement in glucose tolerance observed following VSG. a, Among WT mice, fasting blood glucose is reduced following VSG, whereas among KO mice it is increased. **b, c**, Among WT mice, VSG improves the excursion of blood glucose following an i.p. bolus of $1\,g\,kg^{-1}$ dextrose; among KO mice, the glucose tolerance of VSG and sham-operated mice is equivalent. AUC, area under the curve. Data are shown as mean $\pm$ s.e. $*P < 0.05$, $**P < 0.01$, $***P < 0.001$. $n = 13$ WT-sham, 10 WT-VSG, 9 KO-sham, 10 KO-VSG.

16S ribosomal RNA gene. Because all the mice in this study were maintained on the same purified HFD, and because the average caloric intake by WT-VSG mice was only reduced in the first 3 weeks of this 14-week study (Fig. 3), any observed differences are unlikely to be secondary to differing caloric intake or macronutrient content of the diet. Moreover, because WT-VSG, KO-sham and KO-VSG mice had equivalent body weights at death, any observed differences among these groups are unlikely to be secondary to differing body weight or composition.

Weighted UniFrac analysis (sensitive to abundances of taxa)[33] showed separation of WT-VSG samples from WT-sham samples along the first principal component, indicating that VSG had a stronger effect on microbiota composition in WT mice than in KO mice (Fig. 5a, Extended Data Fig. 3, two-way ANOVA with Tukey post hoc). As shown in Fig. 5b, c, the separation of samples in the principal components analysis plot reflects differences in the Bacteroidetes and Firmicutes levels. In light of these differences, we further identified specific taxonomic changes that result from an interaction between genotype and surgery, as these may represent microbial groups that are critical to the potent effects of bariatric surgery—though future studies involving colonization of germ-free mice would be required for definitive evidence supporting a functional involvement.

The relative abundance of several bacteria previously identified as important modulators of systemic metabolism was altered differently by VSG according to genotype. Specifically, the relative abundance of *Bacteroides* was substantially reduced in WT-VSG mice relative to WT-sham controls, but did not vary with surgery among KO mice (Fig. 5d, two-way ANOVA with Tukey post hoc, $P < 0.05$). A recent study investigating the therapeutic potential of probiotic treatment in obese women found that decreasing prevalence of *Bacteroides* was associated with decreasing adiposity and improved glucose control[34]. Likewise, in the present study, decreasing abundance of *Bacteroides* was associated with decreased weight gain, fat gain (Extended Data Fig. 4), and decreased AUC in a glucose tolerance test—suggesting a functional association that depends on FXR.

An uncharacterized genus in the Porphyromonadaceae family, a bacterial group negatively correlated with type-1 diabetes[35], and decreased in HFD-fed mice[22], was substantially increased in WT-VSG mice relative to WT-sham controls. In contrast, this group was reduced in KO-VSG mice relative to their sham-operated controls (Fig. 5e, two-way ANOVA with Tukey post hoc, $P < 0.05$).

Finally, the relative abundance of *Roseburia* was 12-fold higher in WT-VSG caeca compared to WT-sham, but the abundance of this microbe in both KO groups resembled the WT-sham group (Fig. 5f, two-way ANOVA with Tukey post hoc, $P < 0.05$). Importantly, and consistent with our findings, two recent gut metagenome analyses identified decreased abundance of *Roseburia* as highly discriminant for type-2 diabetes mellitus, in both a European and a Chinese population[36,37].

Likewise, a study investigating the therapeutic effect of a prebiotic treatment in rodents found that increased abundance of *Roseburia* was associated with weight loss and improved glucose tolerance, independent of food intake[38]. In the present study, the abundance of *Roseburia* was negatively correlated with AUC in the glucose tolerance test (Extended Data Fig. 4), and this was due primarily to the relationship within the WT-VSG group ($R^2 = 0.75$, $P < 0.05$, Fig. 5g), suggesting an FXR-dependent functional association.

In addition, we observed genotype-independent changes in the relative abundance of the genera *Lactobacillus* and *Lactococcus* and of Enterobacteriaceae (Extended Data Fig. 5). Consistent with this, an increase in *Escherichia coli* and other enterobacteria has likewise been reported after RYGB[23,24,26]. Such changes may indeed contribute to the benefits of VSG and other bariatric procedures, but the present data suggest they are not sufficient to elicit improvements in energy balance and glucose homeostasis.

Changes in gut microbiota may influence host metabolism in part due to the ability of the microbiota to attain colonic dietary conversion, resulting mostly in the production of fatty acid end products. Pertinent to this, a wide range of data now links the production of short-chain fatty acids (SCFAs) to various metabolic outcomes[36,37,39,40]. To this end, we measured caecal SCFAs and other organic acids produced by the gut microbiota. There were no differences in the total abundance of SCFAs among the four groups (Extended Data Table 1). The relative abundances of butyrate and propionate (Extended Data Fig. 6a, b), but not acetate (Extended Data Fig. 6c) were altered by VSG and this did not differ between genotypes (two-way ANOVA with Tukey post hoc, $P < 0.05$). The resulting decrease in the acetate:butyrate ratio (Extended Data Fig. 6d, two-way ANOVA with Tukey post hoc, $P < 0.001$) possibly indicates that acetate is more efficiently converted to butyrate following VSG. Consistent with the increase in *Lactobacillus* and *Lactococcus*, we also observed an increase in lactate following VSG (Extended Data Table 1). Again, although such changes may indeed contribute to the benefits of VSG and other bariatric procedures, the present data suggest they are not sufficient to elicit metabolic improvements.

Discussion

Though a number of local physiological and environmental variables may be altered by VSG, here we have identified a critical role for altered bile acid signalling. Taken together, the present results demonstrate that a functional FXR pathway is necessary for sustained weight loss, suppression of rebound hyperphagia and improved glucose control following VSG. Importantly, KO mice have an equivalently small stomach, yet they do not demonstrate the same improvements as WT mice. Thus our findings directly contradict the common assumption that mechanical restriction, resulting from the reduced stomach size, is sufficient to mediate the therapeutic effects of VSG.
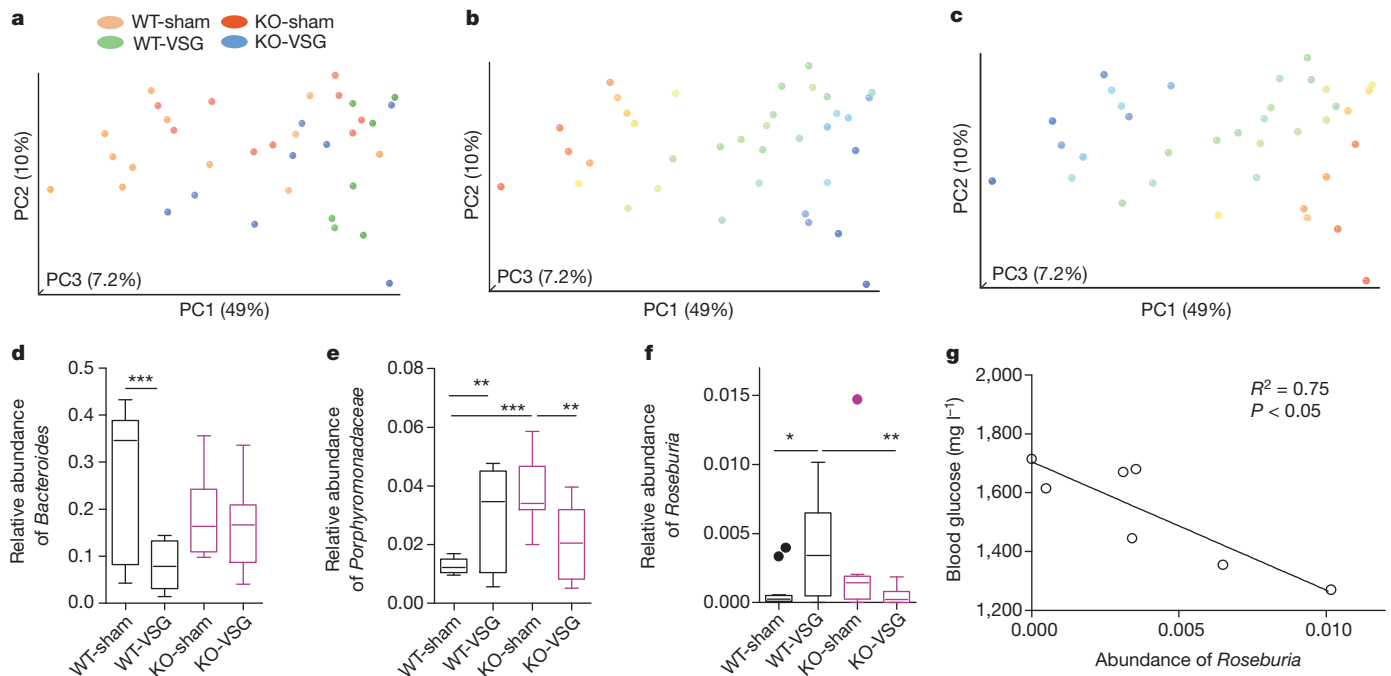
Figure 5 | VSG and FXR alter the composition of caecal microbial communities. a, Principal coordinates analysis plot of weighted UniFrac distances. Each dot represents a caecal community with the various surgical/genotype groups indicated by colour. The percentage of variation explained by each principal coordinate (PC1, PC2, PC3) is shown in parentheses. **b, c,** Abundance gradient of Bacteroidetes (**b**) and Firmicutes (**c**). Each dot is in the same position as it was in **a** but the colour now indicates the relative abundance (blue indicating low abundance to red indicating high abundance) of Bacteroidetes and Firmicutes respectively. **d,** Relative abundance of *Bacteroides* was reduced in WT-VSG compared to WT-sham operated mice,

but did not differ in KO mice. **e,** Relative abundance of one genus in the Porphyromonadaceae family was increased in WT-VSG compared to WT-sham operated mice, but was reduced in KO-VSG mice relative to KO-sham operated controls. **f,** Relative abundance of *Roseburia* was increased in WT-VSG compared to WT-sham operated mice, but did not differ in KO mice; individual data points show outliers. **g,** Among WT-VSG mice, the relative abundance of *Roseburia* was tightly correlated with fasting blood glucose. Data are presented as Tukey box-plots. *$P < 0.05$, **$P < 0.01$, ***$P < 0.001$. $n = 12$ WT-sham, 7 WT-VSG, 9 KO-sham, 8 KO-VSG.

In agreement with this, FXR-signalling is implicated in the regulation of lipid and glucose metabolism[41–44]. Initial reports emphasized a protective role, concluding that FXR signalling is necessary for normal glucose homeostasis. FXR KO mice exhibit impaired glucose and insulin tolerance when maintained on a chow diet[41,42], despite modestly elevated plasma bile acids. In apparent contrast, however, they are resistant to HFD-induced obesity and glucose intolerance[18]. Intriguingly, two studies investigating the effect of the synthetic FXR agonist GW4064 on the development of HFD-induced obesity and glucose intolerance[45,46] yielded opposite results. Whereas Watanabe *et al.*[46] report greater sensitivity to diet-induced metabolic dysfunction, Ma *et al.*[45] report resistance to diet-induced obesity following treatment with GW4064. A major difference between the two studies was route of administration. Watanabe *et al.* delivered the drug orally via the diet, whereas Ma *et al.* delivered it intraperitoneally. FXR is expressed in multiple organs important for the regulation of metabolism, including liver, adipose tissue and intestine, and its activation in these compartments may elicit opposing effects on metabolism, perhaps contributing to this discrepancy. Relevant to this, bile acids may also affect metabolism by signalling via the G-protein-coupled receptor TGR5, raising the possibility of cross-talk between these systems[47]. Finally, we note these contradictory phenotypes have likewise been observed in the complex regulation of gene expression by other members of the nuclear receptor family. The PPARγ haploin-sufficient mouse, for example, is more insulin sensitive despite the fact that PPARγ agonists are well-known for their insulin-sensitizing effects[48]. Like PPARγ, FXR and other nuclear receptors may either activate or repress the transcription of target genes, depending on the presence of co-activator and co-repressor complexes. Therefore, loss-of-FXR function might paradoxically be associated with a relative increased expression in a subset of FXR-regulated genes, while still making the animal

resistant to treatments that activate FXR. This may explain the present conundrum that FXR KO mice are simultaneously resistant to some of the deleterious metabolic effects of consuming a HFD and also relatively unresponsive to the metabolic benefits of VSG.

Bariatric surgical procedures, such as VSG, are currently the most effective therapy for the treatment of obesity and are moreover associated with substantial improvements in co-morbidities, including type-2 diabetes mellitus. The underlying molecular mechanisms contributing to these benefits remain largely undetermined, despite offering tremendous potential to reveal new targets for therapeutic intervention. Progress towards this goal has probably been hindered by a widespread belief that surgery exerts its effects simply by making it physically difficult to consume or absorb calories. The current work provides an alternative framework—that is, it identifies FXR-signalling as a molecular mechanism necessary for both key changes to gut microbial communities and many associated metabolic benefits of VSG. These findings provide a new understanding of the mechanisms that underlie the benefits of bariatric surgery and suggest new targets for developing less-invasive therapeutic interventions.

METHODS SUMMARY

RNA-seq and unbiased pathway analysis. These were performed using RNA collected from the distal small intestine of VSG and sham-operated, pair-fed male (SPF) mice that were the subjects of a previously published study[9].
Animals. Singly-housed FXR KO mice and their WT littermates[49] were allowed *ad libitum* access to a high-fat diet (HFD) and water unless otherwise noted. VSG or sham surgery was performed as described elsewhere[3].
Microbiota. Caecal microbiota composition was analysed by pyrosequencing of the V1-V2 region from the bacterial 16S rRNA gene. PCR amplicons were generated from caecal DNA. Sequence data were analysed by using the QIIME software package (version 1.5.0)[50].

1. Pories, W. J. Bariatric surgery: risks and rewards. *J. Clin. Endocrinol. Metab.* **93**, S89–S96 (2008).
2. Schauer, P. R. *et al.* Bariatric surgery versus intensive medical therapy in obese patients with diabetes. *N. Engl. J. Med.* **366**, 1567–1576 (2012).
3. Wilson-Pérez, H. E. *et al.* Vertical sleeve gastrectomy is effective in two genetic mouse models of glucagon-like peptide-1 receptor deficiency. *Diabetes* **62**, 2380–2385 (2013).
4. Chambers, A. P. *et al.* Weight-independent changes in blood glucose homeostasis after gastric bypass or vertical sleeve gastrectomy in rats. *Gastroenterology* **141**, 950–958 (2011).
5. Karamanakos, S. N., Vagenas, K., Kalfarentzos, F. & Alexandrides, T. K. Weight loss, appetite suppression, and changes in fasting and postprandial ghrelin and peptide-YY levels after Roux-en-Y gastric bypass and sleeve gastrectomy: a prospective, double blind study. *Ann. Surg.* **247**, 401–407 (2008).
6. Stefater, M. A., Wilson-Pérez, H. E., Chambers, A. P., Sandoval, D. A. & Seeley, R. J. All bariatric surgeries are not created equal: insights from mechanistic comparisons. *Endocr. Rev.* **33**, 595–622 (2012).
7. Jackness, C. *et al.* Very low-calorie diet mimics the early beneficial effect of Roux-en-Y gastric bypass on insulin sensitivity and β-cell function in type 2 diabetic patients. *Diabetes* **62**, 3027–3032 (2013).
8. Bradley, D. *et al.* Gastric bypass and banding equally improve insulin sensitivity and β cell function. *J. Clin. Invest.* **122**, 4667–4674 (2012).
9. Myronovych, A. *et al.* Vertical sleeve gastrectomy reduces hepatic steatosis while increasing serum bile acids in a weight-loss-independent manner. *Obesity* **22**, 390–400 (2014).
10. Patti, M. E. *et al.* Serum bile acids are higher in humans with prior gastric bypass: potential contribution to improved glucose and lipid metabolism. *Obesity* **17**, 1671–1677 (2009).
11. Larsson, E. *et al.* Analysis of gut microbial regulation of host gene expression along the length of the gut and regulation of gut microbial ecology through MyD88. *Gut* **61**, 1124–1131 (2012).
12. Lhoste, E. F. *et al.* The human colonic microflora influences the alterations of xenobiotic-metabolizing enzymes by catechins in male F344 rats. *Food Chem. Toxicol.* **41**, 695–702 (2003).
13. Brodziak, F., Meharg, C., Blaut, M. & Loh, G. Differences in mucosal gene expression in the colon of two inbred mouse strains after colonization with commensal gut bacteria. *PLoS ONE* **8**, e72317 (2013).
14. Vijay-Kumar, M. *et al.* Metabolic syndrome and altered gut microbiota in mice lacking Toll-like receptor 5. *Science* **328**, 228–231 (2010).
15. Kohli, R. *et al.* Weight loss induced by Roux-en-Y gastric bypass but not laparoscopic adjustable gastric banding increases circulating bile acids. *J. Clin. Endocrinol. Metab.* **98**, E708–E712 (2013).
16. Cummings, B. P. *et al.* Vertical sleeve gastrectomy improves glucose and lipid metabolism and delays diabetes onset in UCD-T2DM rats. *Endocrinology* **153**, 3620–3632 (2012).
17. Gerhard, G. S. *et al.* A role for fibroblast growth factor 19 and bile acids in diabetes remission after Roux-en-y gastric bypass. *Diabetes Care* **36**, 1859–1864 (2013).
18. Prawitt, J. *et al.* Farnesoid X receptor deficiency improves glucose homeostasis in mouse models of obesity. *Diabetes* **60**, 1861–1871 (2011).
19. Chambers, A. P. *et al.* The effects of vertical sleeve gastrectomy in rodents are ghrelin independent. *Gastroenterology* **144**, 50–52.e5 (2013).
20. Ryan, K. K., Woods, S. C. & Seeley, R. J. Central nervous system mechanisms linking the consumption of palatable high-fat diets to the defense of greater adiposity. *Cell Metab.* **15**, 137–149 (2012).
21. Ley, R. E. *et al.* Obesity alters gut microbial ecology. *Proc. Natl Acad. Sci. USA* **102**, 11070–11075 (2005).
22. Parks, B. W. *et al.* Genetic control of obesity and gut microbiota composition in response to high-fat, high-sucrose diet in mice. *Cell Metab.* **17**, 141–152 (2013).
23. Zhang, H. *et al.* Human gut microbiota in obesity and after gastric bypass. *Proc. Natl Acad. Sci. USA* **106**, 2365–2370 (2009).
24. Furet, J.-P. *et al.* Differential adaptation of human gut microbiota to bariatric surgery-induced weight loss: links with metabolic and low-grade inflammation markers. *Diabetes* **59**, 3049–3057 (2010).
25. Graessler, J. *et al.* Metagenomic sequencing of the human gut microbiome before and after bariatric surgery in obese patients with type 2 diabetes: correlation with inflammatory and metabolic parameters. *Pharmacogenom. J.* **13**, 514–522 (2012).
26. Liou, A. P. *et al.* Conserved shifts in the gut microbiota due to gastric bypass reduce host weight and adiposity. *Sci. Transl. Med.* **5**, 178ra41 (2013).
27. Turnbaugh, P. J. *et al.* An obesity-associated gut microbiome with increased capacity for energy harvest. *Nature* **444**, 1027–1031 (2006).
28. Turnbaugh, P. J., Bäckhed, F., Fulton, L. & Gordon, J. I. Diet-induced obesity is linked to marked but reversible alterations in the mouse distal gut microbiome. *Cell Host Microbe* **3**, 213–223 (2008).
29. Merritt, M. E. & Donaldson, J. R. Effect of bile salts on the DNA and membrane integrity of enteric bacteria. *J. Med. Microbiol.* **58**, 1533–1541 (2009).
30. Islam, K. B. M. S. *et al.* Bile acid is a host factor that regulates the composition of the cecal microbiota in rats. *Gastroenterology* **141**, 1773–1781 (2011).
31. Sayin, S. I. *et al.* Gut microbiota regulates bile acid metabolism by reducing the levels of tauro-β-muricholic acid, a naturally occurring FXR antagonist. *Cell Metab.* **17**, 225–235 (2013).
32. Swann, J. R. *et al.* Systemic gut microbial modulation of bile acid metabolism in host tissue compartments. *Proc. Natl Acad. Sci. USA* **108** (Suppl. 1), 4523–4530 (2011).
33. Lozupone, C. & Knight, R. UniFrac: a new phylogenetic method for comparing microbial communities. *Appl. Environ. Microbiol.* **71**, 8228–8235 (2005).
34. Dewulf, E. M. *et al.* Insight into the prebiotic concept: lessons from an exploratory, double blind intervention study with inulin-type fructans in obese women. *Gut* **62**, 1112–1121 (2013).
35. Wen, L. *et al.* Innate immunity and intestinal microbiota in the development of Type 1 diabetes. *Nature* **455**, 1109–1113 (2008).
36. Qin, J. *et al.* A metagenome-wide association study of gut microbiota in type 2 diabetes. *Nature* **490**, 55–60 (2012).
37. Karlsson, F. H. *et al.* Gut metagenome in European women with normal, impaired and diabetic glucose control. *Nature* **498**, 99–103 (2013).
38. Neyrinck, A. M. *et al.* Dietary modulation of clostridial cluster XIVa gut bacteria (*Roseburia* spp.) by chitin-glucan fiber improves host metabolic alterations induced by high-fat diet in mice. *J. Nutr. Biochem.* **23**, 51–59 (2012).
39. Ridaura, V. K. *et al.* Gut microbiota from twins discordant for obesity modulate metabolism in mice. *Science* **341**, 1241214 (2013).
40. Vrieze, A. *et al.* Transfer of intestinal microbiota from lean donors increases insulin sensitivity in individuals with metabolic syndrome. *Gastroenterology* **143**, 913–6.e7 (2012).
41. Cariou, B. *et al.* The farnesoid X receptor modulates adiposity and peripheral insulin sensitivity in mice. *J. Biol. Chem.* **281**, 11039–11049 (2006).
42. Ma, K., Saha, P. K., Chan, L. & Moore, D. D. Farnesoid X receptor is essential for normal glucose homeostasis. *J. Clin. Invest.* **116**, 1102–1109 (2006).
43. Zhang, Y. *et al.* Activation of the nuclear receptor FXR improves hyperglycemia and hyperlipidemia in diabetic mice. *Proc. Natl Acad. Sci. USA* **103**, 1006–1011 (2006).
44. Porez, G., Prawitt, J., Gross, B. & Staels, B. Bile acid receptors as targets for the treatment of dyslipidemia and cardiovascular disease. *J. Lipid Res.* **53**, 1723–1737 (2012).
45. Ma, Y., Huang, Y., Yan, L., Gao, M. & Liu, D. Synthetic FXR agonist GW4064 prevents diet-induced hepatic steatosis and insulin resistance. *Pharm. Res.* **30**, 1447–1457 (2013).
46. Watanabe, M. *et al.* Lowering bile acid pool size with a synthetic farnesoid X receptor (FXR) agonist induces obesity and diabetes through reduced energy expenditure. *J. Biol. Chem.* **286**, 26913–26920 (2011).
47. Thomas, C., Pellicciari, R., Pruzanski, M., Auwerx, J. & Schoonjans, K. Targeting bile-acid signalling for metabolic diseases. *Nature Rev. Drug Discov.* **7**, 678–693 (2008).
48. Miles, P. D., Barak, Y., He, W., Evans, R. M. & Olefsky, J. M. Improved insulin-sensitivity in mice heterozygous for PPAR-γ deficiency. *J. Clin. Invest.* **105**, 287–292 (2000).
49. Sinal, C. J. *et al.* Targeted disruption of the nuclear receptor FXR/BAR impairs bile acid and lipid homeostasis. *Cell* **102**, 731–744 (2000).
50. Caporaso, J. G. *et al.* QIIME allows analysis of high-throughput community sequencing data. *Nature Methods* **7**, 335–336 (2010).

Author Contributions K.K.R. conceptualized, designed, performed and analysed the experiments and wrote the manuscript. C.C., A.M., H.E.W.-P., D.A.S. and R. Kohli performed experiments and edited the manuscript. R. Karns performed the bioinformatics analysis of the RNA-seq data. V.T. and F.B. designed and performed the microbiota analysis and edited the manuscript. P.K.-D. and F.B. designed and performed the analysis of caecal metabolites and edited the manuscript. R.J.S. conceptualized, designed and analysed the experiments and wrote the manuscript.

Author Information Raw and normalized RNA-seq data have been deposited in the NCBI Gene Expression Omnibus database under accession number GSE53782. Reprints and permissions information is available at www.nature.com/reprints. The authors declare competing financial interests: details are available in the online version of the paper. Readers are welcome to comment on the online version of the paper. Correspondence and requests for materials should be addressed to R.J.S. (randy.seeley@uc.edu).

METHODS

Protocols. The Institutional Animal Care and Use Committees at the University of Cincinnati and Cincinnati Children's Hospital Medical Center approved all animal protocols.

RNA-seq and unbiased pathway analysis. For RNA-seq followed by unbiased pathway analysis, the distal 1.5 cm of small intestine was collected from 5 VSG and 5 sham-operated, pair-fed male (SPF) C57Bl/6J mice (Jackson Labs, BarHarbour, ME) that were the subjects of a previously published study[9]. See ref. 9 for further methodological detail. RNA-seq libraries prepared with the Illumina TruSeq RNA preparation kit were sequencing on an Illumina Hi-Seq 2000, with single-end 50 bp reads. Analysis was performed in GeneSpring NGS (Agilent Technologies, Santa Clara, CA), where sequences were aligned to the mm9 reference mouse genome and assigned Ensembl annotations. Aligned gene reads that passed quality controls (quality threshold ≥30, zero Ns allowed, no multiply mapping reads) were quantified and used to calculated reads per kilobase per million (RPKM). Raw data were normalized using the DeSeq algorithm where reads were thresholded to a minimum read count of 1. An additional filter required at least 10 reads per entity in each sample of either VSG or SPF samples ($N = 14{,}591$ entities). Differentially expressed genes with a fold change of ≥1.5 between VSG and SPF animals ($N = 882$) were submitted to pathway analysis, which assessed significance of overlap between the 882 differential genes and those genes in pathways curated by Wikipathways, BioCyc, BioPax and Legacy, with a P-value cut-off of 0.05.

Surgery. VSG surgery was performed in DIO mice using isofluorane anaesthesia. The lateral 80% of the stomach was excised leaving a tubular gastric remnant in continuity with the oesophagus superiorly and the pylorus and duodenum inferiorly. The sham procedure involved analogous isolation of the stomach followed by manually applying pressure with blunt forceps along a vertical line between the oesophageal sphincter and the pylorus. Mice consumed liquid diet (Osmolite OneCal) for the first 3 post-operative days, and were re-introduced to HFD on day 3.

Mice. 10–12-week-old male FXR KO mice and their WT littermates, described elsewhere[49] and bred from founders acquired from the Jackson Labs (Bar Harbour, ME), were singly housed in an AAALAC-approved facility with a 12–12 light–dark cycle, and allowed *ad libitum* access to HFD (D12492, Research Diets, New Brunswick, NJ) and water unless otherwise noted. After 10 weeks of HF-feeding, male mice were randomly divided into body weight and fat-matched groups within genotype, and we performed VSG or sham surgery as above. Based on our power analyses, completed using previous data to determine the expected variance and effect sizes, and based on our historical data regarding post-operative mortality, we performed sham surgery on 13 WT and 9 KO mice and VSG surgery on 14 WT and 15 KO mice. 5 KO-VSG and 4 WT-VSG mice died from complications of surgery and were not included in any of the analyses. Food intake and body weight was monitored weekly. Body composition was measured 1 week before and 11 weeks following surgery by magnetic resonance imaging (Echo Medical Systems, Houston, TX). An additional 1 WT-sham, 2 KO-VSG and 2 WT-VSG mice died (or were found moribund) during the period of metabolic phenotyping that occurred between weeks 8 and 15. For any given analysis, only mice that are represented throughout the entire timecourse were included. In addition, for the macronutrient preference study, data from several individuals were excluded based on pre-established criteria—in this case, that the mice consistently spilled the powdered macronutrient diets on the cage floor making accurate measurement of what was ingested impossible. For the microbiota analyses, one WT-VSG individual was excluded due to a noted investigator error while collecting the caecal samples at sacrifice. Investigators conducting the gene expression and microbiota analyses were blind to the experimental groups.

Macronutrient preference. Food choice was assayed during postoperative week 10 using a macronutrient selection paradigm, in which 3 pure macronutrient diets (Harlan Teklad; TD.02521 (carbohydrate), TD.02522 (fat) and TD02523 (protein)) were presented simultaneously in separate containers for 6 days ($n = 12$ WT-sham, 6 WT-VSG, 8 KO-sham, 7 KO-VSG).

Glucose tolerance tests. Glucose tolerance was assayed during postoperative week 8 in 5-h fasted mice. Blood glucose was measured with AccuCheck meters and strips (Roche, Indianapolis, IN) from the tip of the tail vein in unrestrained animals at baseline, and at regular intervals following an i.p. injection of $1 \, \mathrm{g \, kg^{-1}}$ body weight dextrose ($n = 13$ WT-sham, 10 WT-VSG, 9 KO-sham, 10 KO-VSG).

Analysis of gut microbial communities. Whereas much of the microbiota is dead in the faeces, the caecum is an active bioreactor with high metabolic fermentative capacity. Thus we focused our study on the caecal microbiota. Caecal microbiota composition was analysed by pyrosequencing of the V1-V2 region from the bacterial 16S rRNA gene. PCR amplicons were generated from caecal DNA obtained from WT and FXR KO mice that underwent either VSG or sham operations ($n = 12$ WT-sham, 7 WT-VSG, 9 KO-sham, 8 KO-VSG). Sequence data were analysed by using the QIIME software package (version 1.5.0)[50].

Sample processing, extraction of genomic DNA and amplification for 454 pyrosequencing. Aliquots of caecal material were collected and immediately frozen in liquid nitrogen. These aliquots were stored at $-80 \, ^{\circ}\mathrm{C}$ until extracted: approximately half of each aliquot was used for isolation of genomic DNA and the other half was used for extraction of SCFAs and microbial metabolites.

Genomic DNA was isolated from 50–80 mg of caecal content using the repeated bead beating (RBB) method previously described by Salonen *et al.*[51]. The V1-V2 region of the 16 rRNA gene was amplified using the 27F and 338R primers fused with 454 Titanium sequencing adapters. 338R primers contained unique error-correcting 12-base barcodes that allow to tag PCR products from different samples[52]. Each sample was amplified in triplicate in a reaction volume of 25 µl containing 1.5 U of FastStart Taq DNA Polymerase (Roche), 0.2 µM of each primer and 10–20 ng of genomic DNA. PCR was carried out under the following conditions: initial denaturation for 3 min at 95 °C, followed by 25 cycles of denaturation for 20 s at 95 °C, annealing for 20 s at 52 °C and elongation for 60 s at 72 °C, and a final elongation step for 8 min at 72 °C. Triplicates were combined, purified with the NucleoSpin Gel and PCR Clean-up kit (Macherey-Nagel, Germany) and then quantified using the Quant-iT PicoGreen dsDNA kit (Invitrogen, Carlsbad, CA). Purified PCR products were diluted to a concentration of 20 ng µl^{-1} and pooled in equal amounts. The pooled amplicons were purified again with the Ampure magnetic purification beads (Agencourt, Danvers, MA) to remove short amplification products. Sequencing was performed using 454 GS FLX titanium chemistry at GATC Biotech (Konstanz, Germany).

Analysis of 16S rRNA gene sequences. Raw data were quality filtered to remove sequences that were shorter than 200 nucleotides, longer than 1,000 nucleotides, contained primer mismatches, ambiguous bases, uncorrectable barcodes, or homopolymer runs in excess of six bases. Quality filtered reads were trimmed of 454 adaptor and barcode sequences, and were analysed with the software package Quantitative Insights Into Microbial Ecology (QIIME)[50] (version 1.5.0). A total of 376,965 sequences were obtained for 36 samples; sequences were demultiplexed and an average of 10,471 sequences were attributed to each sample (range: 7,208–12,522 sequences).

Sequences were assigned to operational taxonomic units (OTUs) using UCLUST with a 97% threshold of pairwise identity. The most abundant sequence was picked as representative for each OTU and was given taxonomic assignment using the Ribosomal Database Project (RDP) Classifier[4]. Representative OTUs were aligned using Pynast[53] and used to build a phylogenetic tree with FastTree[54], which was used to estimate β-diversity of samples (weighted UniFrac[33]). Sequences were checked for chimaeras using ChimeraSlayer and chimaeric sequences were excluded from all downstream analyses. Similarly, singletons and sequences that could not be aligned with Pynast were also excluded.

Extraction of microbial metabolites (SCFAs and other organic acids). GC-MS was used for measurement of organic acids in mouse caecal samples ($n = 12$ WT-sham, 7 WT-VSG, 9 KO-sham, 8 KO-VSG). After extraction with diethyl ether, an aliquot of each sample was derivatized with N-tert-butyldimethylsilyl-N-methyltrifluoroacetamide (MTBSTFA; Sigma), and the organic acids were quantified by using a gas chromatograph (Model 7890 A, Agilent Technologies) coupled to a mass spectrometer detector (Model 5975 C, inert XL MSD with triple Axis Detector; Agilent Technologies). 50–80 mg of frozen caecal contents were transferred to glass tubes (16 × 125 mm) fitted with a screw cap, and a volume of 100 µl of internal standards stock solution ($[1\text{-}^{13}\mathrm{C}]$acetate and $[^2\mathrm{H}_6]$propionate 1 M, $[^{13}\mathrm{C}_4]$butyrate 0.5 M, $[1\text{-}^{13}\mathrm{C}_1]$isobutyrate and $[1\text{-}^{13}\mathrm{C}]$isovalerate 0.1 M, $[1{,}2\text{-}^{13}\mathrm{C}_2]$hexanoate, $[^{13}\mathrm{C}]$lactate and $[^{13}\mathrm{C}_4]$succinic acid each at 40 mM) was added to the tubes. Prior to extraction samples were freeze-dried at $-50 \, ^{\circ}\mathrm{C}$ for 3 h (yield 8–15 mg dry weight). After acidification with 50 µl of 37% HCl, the organic acids were extracted twice in 2 ml of diethyl ether. A 500 µl aliquot of the extracted sample was mixed together with 50 µl of MTBSTFA (Sigma) at room temperature. An aliquot (1 µl) of the resulting derivatized material was injected into a gas chromatograph (Agilent Technologies 7890 A) coupled to a mass spectrometer detector (Agilent Technologies 5975 C). A linear temperature gradient was used: the initial temperature of 65 °C was held for 6 min, increased to 260 °C ($15 \, ^{\circ}\mathrm{C \, min^{-1}}$) and then to 280 °C for 5 min. The injector and transfer line temperatures were 250 °C. Quantitation was completed in selected ion monitoring acquisition mode by comparison to labelled internal standards (valerate was compared to $[1\text{-}^{13}\mathrm{C}]$isovalerate, heptanoate and octanoate were compared to $[1{,}2\text{-}^{13}\mathrm{C}_2]$hexanoate and fumarate was compared to $[^{13}\mathrm{C}_4]$succinic acid). The m/z ratios of monitored ions were as follows: 117 (acetic acid), 131 (propionic acid), 145 (butyric acid), 146 (isovaleric acid), 159 (isovaleric acid and valeric acid, 173 (hexanoic acid), 187 (heptanoic acid), 201 (octanoic acid), 261 (lactic acid), 287 (fumaric acid), 289 (succinic acid), 121 ($[^2\mathrm{H}_2]$- and $[1\text{-}^{13}\mathrm{C}]$acetate), 136 ($[^2\mathrm{H}_5]$propionate), 146 ($[1\text{-}^{13}\mathrm{C}_1]$isobutyrate), 149 ($[^{13}\mathrm{C}_4]$butyrate), 160 ($[1\text{-}^{13}\mathrm{C}]$isovalerate), 175 ($[1{,}2\text{-}^{13}\mathrm{C}_2]$hexanoate), 264 ($[^{13}\mathrm{C}]$lactate) and 293 ($[^{13}\mathrm{C}_4]$succinic acid).

Statistical analyses. Data are presented as mean ± standard errors or as Tukey box-plots, as noted. Data were analysed using the appropriate ANOVA or repeated measures ANOVA (RM ANOVA), followed by Tukey's post-hoc tests, or by *t*-test as indicated. The data were tested for normality and homogeneity of variance. In cases where the data failed these assumptions, the analyses were also done after rank transformation. In no cases did this alter the statistical significance or interpretation of the findings, so the statistics reported in the figures are from the non-transformed analyses. Data were analysed using Prism (Graph Pad, San Diego CA) or Sigma Stat (SYSTAT, San Jose CA) software with the critical value, α, set at $P < 0.05$.

51. Salonen, A. *et al.* Comparative analysis of fecal DNA extraction methods with phylogenetic microarray: effective recovery of bacterial and archaeal DNA using mechanical cell lysis. *J. Microbiol. Methods* **81,** 127–134 (2010).
52. Hamady, M., Walker, J. J., Harris, J. K., Gold, N. J. & Knight, R. Error-correcting barcoded primers for pyrosequencing hundreds of samples in multiplex. *Nature Methods* **5,** 235–237 (2008).
53. Caporaso, J. G. *et al.* PyNAST: a flexible tool for aligning sequences to a template alignment. *Bioinformatics* **26,** 266–267 (2010).
54. Price, M. N., Dehal, P. S. & Arkin, A. P. FastTree: computing large minimum evolution trees with profiles instead of a distance matrix. *Mol. Biol. Evol.* **26,** 1641–1650 (2009).
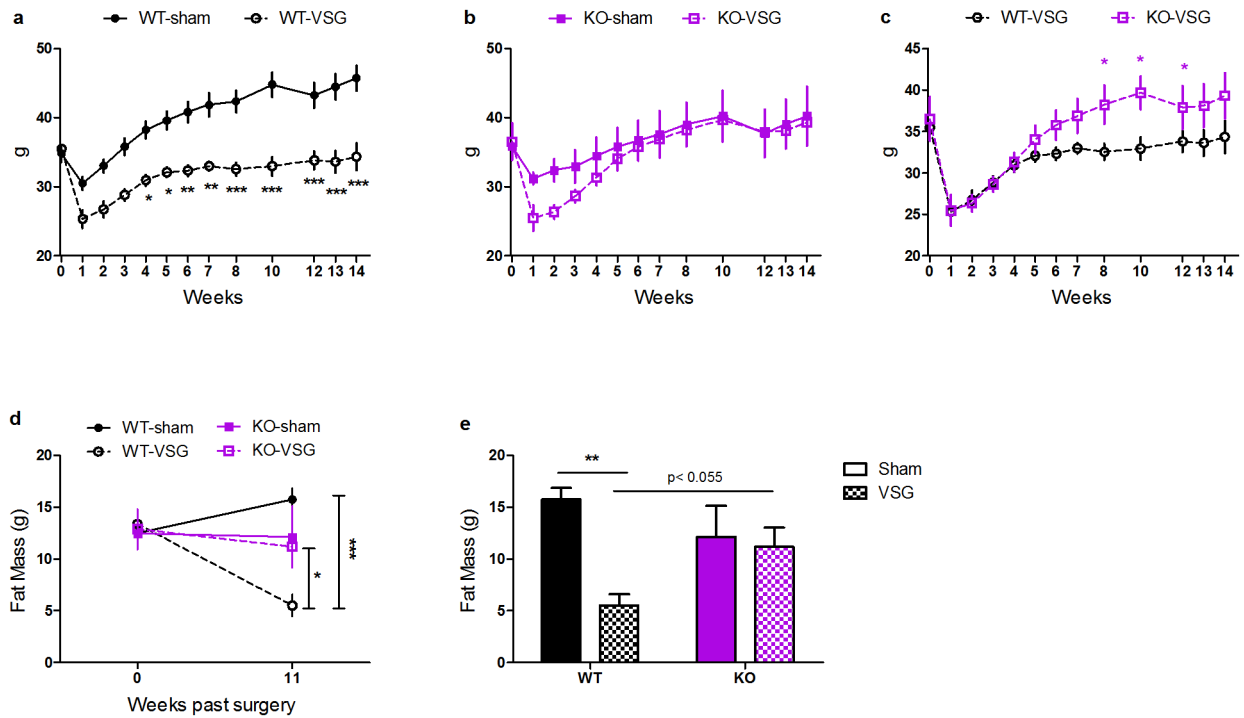
Extended Data Figure 1 | Body weight and body fat in a weight-matched subset of WT and FXR KO mice. These post-hoc analyses include the lightest 9 WT and heaviest 8 FXR-KO mice before surgery, creating 4 well-matched groups. **a–d**, In this subset, WT-VSG lose weight relative to WT-sham controls, and maintain this weight loss for 14 weeks (**a**), whereas KO-VSG mice lose weight initially, but recover to match the weight of KO-sham controls within 4–5 weeks (**b**). Consequently, by week 8 KO-VSG mice were heavier than WT-VSG mice (**c**). Likewise, these groups were well-matched for pre-surgical body fat (**d**). At 11 weeks after surgery, WT-VSG mice had significantly less body fat compared to both WT-sham controls and KO-VSG mice. KO-sham and KO-VSG mice had equivalent adiposity (**e**). Data are shown as mean ± s.e. $*P < 0.05$, $**P < 0.01$, $***P < 0.001$. For all panels $n = 5$ WT-sham, 4 WT-VSG, 4 KO-sham, 4 KO-VSG.
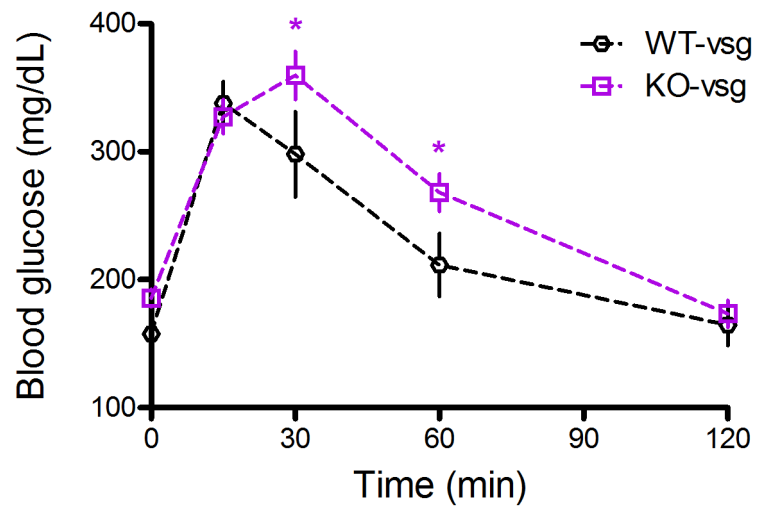
Extended Data Figure 2 | Glucose tolerance in WT-VSG and KO-VSG mice. When the glucose excursion of WT-VSG and KO-VSG mice are compared directly, KO-VSG mice exhibit significantly impaired glucose clearance at both 30 and 60 min. Data are shown as mean ± s.e. *$P < 0.05$. $n = 10$ per group.
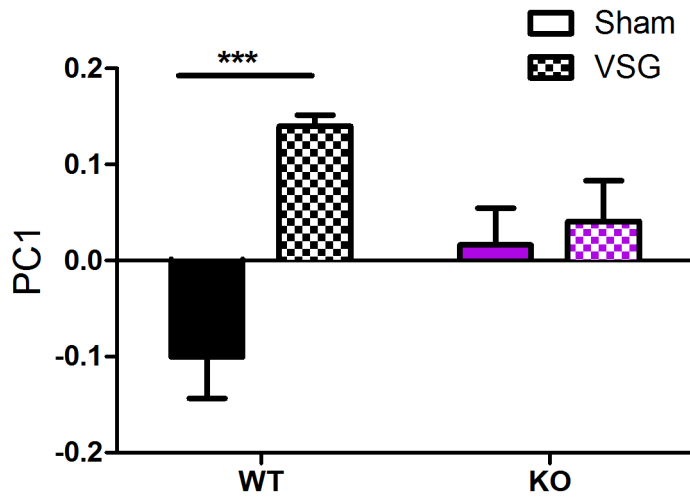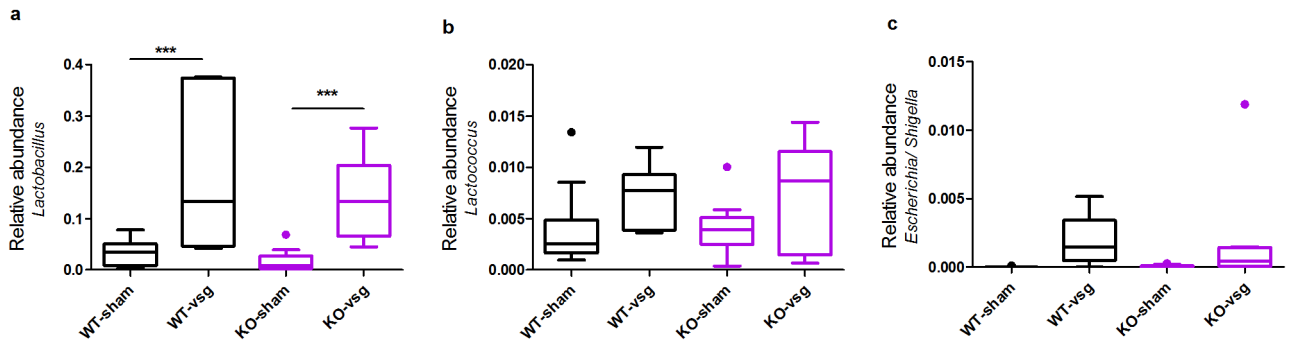
Extended Data Figure 3 | Effect of genotype and VSG on distribution along PC1. Among WT mice, sham and VSG mice separate significantly along PC1. In contrast, among KO mice there is no significant difference between sham and VSG. Data are shown as mean ± s.e. ***$P < 0.001$. $n = 12$ WT-sham, 7 WT-VSG, 9 KO-sham, 8 KO-VSG.
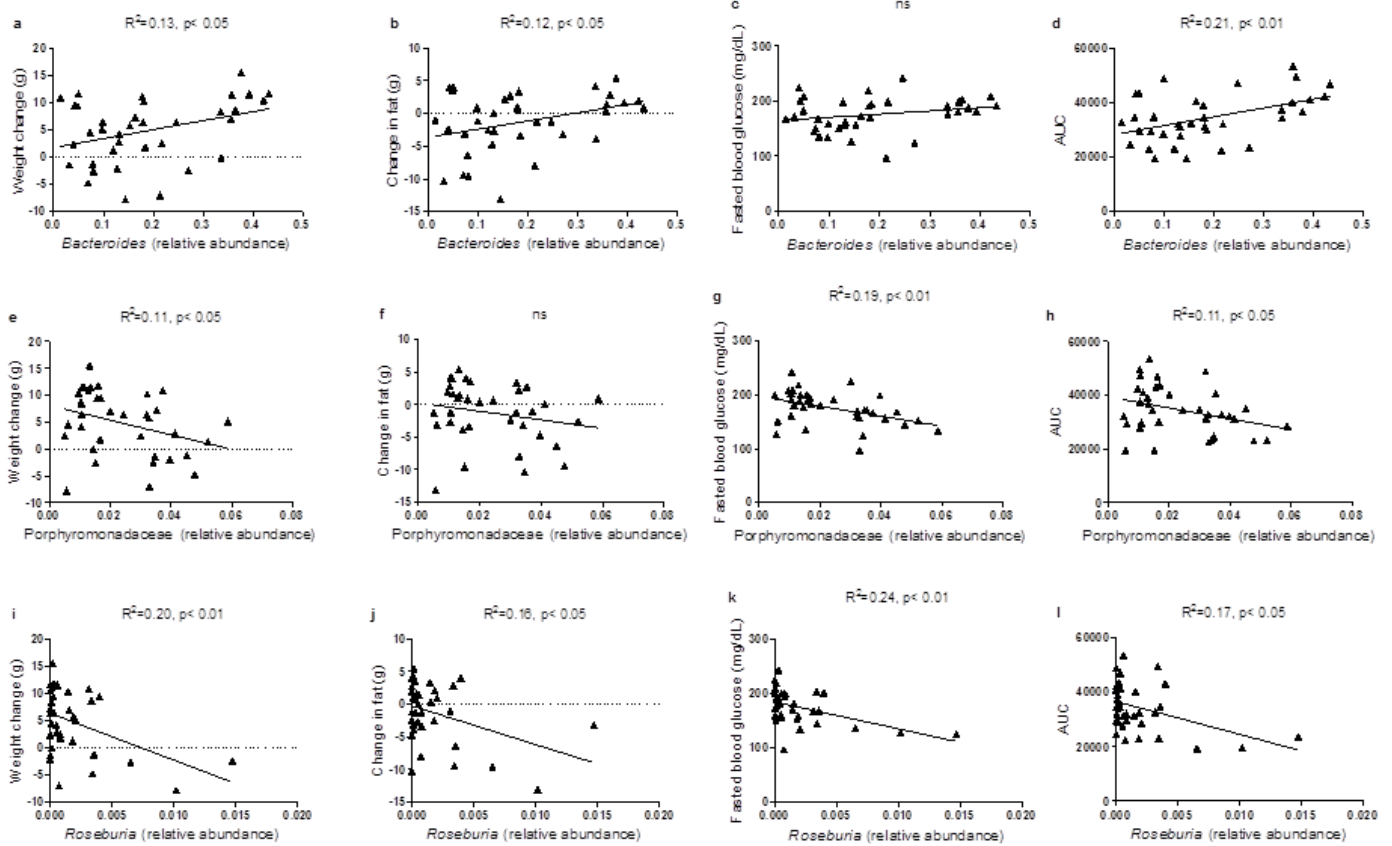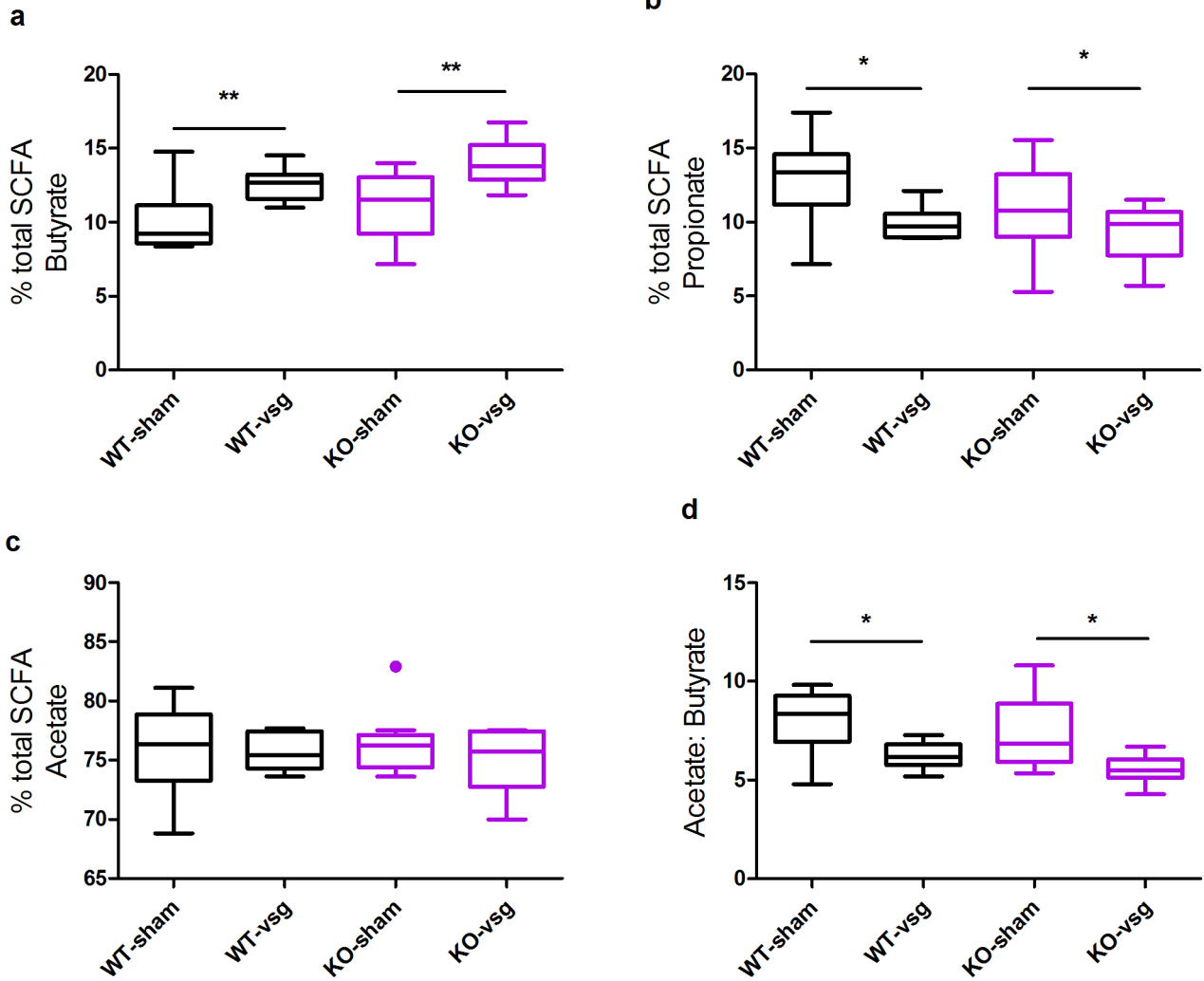
Extended Data Figure 4 | Relative abundance of *Bacteroides*, an uncharacterized genus in Porphyromonadaceae, and *Roseburia* correlated with metabolic parameters. a–d, The relative abundance of *Bacteroides* was significantly correlated with change in body weight (**a**), change in body fat (**b**), and the area under the curve (AUC) in the glucose tolerance test (**d**), but not with fasting blood glucose (**c**). **e–h,** The relative abundance of an uncharacterized genus in Porphyromonadaceae was significantly correlated with change in body weight (**e**), fasting blood glucose (**g**) and AUC in the glucose tolerance test (**h**), but not with change in body fat (**f**). **i–l,** The relative abundance of *Roseburia* was significantly correlated with change in body weight (**i**), change in body fat (**j**), fasting blood glucose (**k**) and AUC in the glucose tolerance test (**l**). $n = 36$.

Extended Data Figure 5 | Effect of genotype and VSG on the relative abundance of *Lactobacillus, Lactococcus* and *Escherichia*. a–c, VSG was associated with a significant increase in the relative abundance of *Lactobacillus* (**a**), *Lactococcus* (**b**) and *Escherichia/Shigella* (**c**) that did not vary according to genotype. Data are presented as Tukey box-plots. $n = 12$ WT-sham, 7 WT-VSG, 9 KO-sham, 8 KO-VSG.

Extended Data Figure 6 | VSG alters the abundance of caecal SCFAs.
a–c, The relative concentration of butyrate (**a**) and propionate (**b**), but not acetate (**c**), was altered by VSG, and this did not differ depending on genotype.

d, The acetate:butyrate ratio is increased following VSG. Data are presented as Tukey box-plots. *$P < 0.05$, **$P < 0.01$. Also see Extended Data Table 1. $n = 12$ WT-sham, 7 WT-VSG, 9 KO-sham, 8 KO-VSG.

Extended Data Table 1 | The effect of VSG on caecal organic acids

Organic acid	WT-Sham	WT-VSG	KO-Sham	KO-VSG	p-value (2-way ANOVA)
Acetate (µmol/g)	142.33 ± 20.45	153.46 ± 26.77	124.54 ± 23.61	160.86 ± 25.04	ns
Propionate (µmol/g)	24.80 ± 3.28	19.60 ± 4.29	15.14 ± 3.78	20.32 ± 4.01	ns
Isobutyrate (µmol/g)	9.56 ±1.71	10.41 ± 2.24	9.11 ± 1.98	10.09 ± 2.09	ns
Butyrate (µmol/g)	19.20 ± 3.42	24.75 ± 4.48	17.55 ± 3.95	29.79 ± 4.19	p (surgery) < 0.05
Isovalerate (µmol/g)	6.25 ± 0.99	7.02 ± 1.3	5.78 ± 1.14	7.08 ± 1.21	ns
Valerate (µmol/g)	2.50 ± 0.41	2.77 ± 0.54	2.19 ± 0.41	2.99 ± 0.41	ns
Hexanoate (µmol/g)	1.14 ± 0.37	1.73 ± 0.49	0.79 ± 0.43	1.74 ± 0.46	ns
Hepthanoate (µmol/g)	0.0080 ± 0.0027	0.0088 ± 0.0027	0.0032 ± 0.0032	0.0088 ± 0.0036	ns
Octanoate (µmol/g)	0.013 ± 0.0056	0.027 ± 0.0073	0.0073 ± 0.0064	0.019 ± 0.0068	ns
Lactate (µmol/g)	13.63 ± 14.80	75.76 ± 19.38	6.95 ± 17.10	38.20 ± 18.13	p (surgery) < 0.01
Succinate (µmol/g)	4.29 ± 2.01	4.55 ± 2.63	5.17 ± 2.32	8.81 ± 2.46	ns
Fumarate (µmol/g)	0.50 ± 0.23	0.82 ± 0.30	0.91 ± 0.27	1.16 ± 0.28	ns
Total SCFAs (C2-C4)	186.33 ± 26.50	197.82 ± 34.70	157.23 ± 30.60	210.99 ± 32.46	ns

Breakdown of the caecal organic acids (µmol per g dry weight) in both WT and KO mice after either sham or VSG surgery.